



HAL
open science

Oxygen Reduction Reaction Mechanism and Kinetics on M-N_xC_y and M@N-C Active Sites Present in Model M-N-C Catalysts Under Alkaline and Acidic Conditions

Ricardo Sgarbi, Kavita Kumar, Frederic Jaouen, Andrea Zitolo, Edson Ticianelli, Frédéric Maillard

► To cite this version:

Ricardo Sgarbi, Kavita Kumar, Frederic Jaouen, Andrea Zitolo, Edson Ticianelli, et al.. Oxygen Reduction Reaction Mechanism and Kinetics on M-N_xC_y and M@N-C Active Sites Present in Model M-N-C Catalysts Under Alkaline and Acidic Conditions. *Journal of Solid State Electrochemistry*, 2021, 25 (1), pp.45-56. <10.1007/s10008-019-04436-w>. <hal-02397015>

HAL Id: hal-02397015

<https://hal.science/hal-02397015v1>

Submitted on 6 Dec 2019

HAL is a multi-disciplinary open access archive for the deposit and dissemination of scientific research documents, whether they are published or not. The documents may come from teaching and research institutions in France or abroad, or from public or private research centers.

L'archive ouverte pluridisciplinaire HAL, est destinée au dépôt et à la diffusion de documents scientifiques de niveau recherche, publiés ou non, émanant des établissements d'enseignement et de recherche français ou étrangers, des laboratoires publics ou privés.



HAL Authorization

[Click here to view linked References](#)

Oxygen Reduction Reaction Mechanism and Kinetics on $M-N_xC_y$ and $M@N-C$ Active Sites Present in Model M-N-C Catalysts Under Alkaline and Acidic Conditions

Ricardo Sgarbi^{a, b}, Kavita Kumar^b, Frédéric Jaouen^{c*}, Andrea Zitolo^d, Edson Ticianelli^a and Frédéric Maillard^{b*}

^a Instituto de Química de São Carlos, Universidade de São Paulo, 13560-960 Sao Carlos, SP, Brazil

^b Univ. Grenoble Alpes, Univ. Savoie Mont Blanc, CNRS, Grenoble INP, LEPMI, 38000 Grenoble, France

^c CNRS, Université de Montpellier, ENSCM, UMR 5253 Institut Charles Gerhardt Montpellier, 2 place Eugène Bataillon, F-34095 Montpellier, France

^d Synchrotron SOLEIL, L'orme des Merisiers, BP 48 Saint Aubin, 91192 Gif-sur-Yvette, France

*Corresponding authors.

E-mail addresses: frederic.maillard@lepmi.grenoble-inp.fr (Frédéric Maillard), frederic.jaouen@umontpellier.fr (Frédéric Jaouen)

ORCID

Ricardo Sgarbi: 0000-0002-1337-9596

Frédéric Jaouen: 0000-0001-9836-3261

Andrea Zitolo: 0000-0002-2187-6699

Edson Ticianelli: 0000-0003-3432-2799

Frédéric Maillard: 0000-0002-6470-8900

Abstract

M-N-C electrocatalysts (where M is Fe or Co) have been investigated for mitigating the dependence on noble metals when catalyzing the oxygen reduction reaction (ORR) for fuel cell technologies in acidic or alkaline conditions. Rotating disc and rotating ring-disk electrodes measurements for Fe-N-C and Co-N-C catalysts demonstrate promising performances and stability for the ORR, while the activity of main suspected active sites ($M-N_xC_y$ and $M@N-C$) has been discussed on the basis of the known physical-chemical properties of the catalysts in acid and alkaline media. Thereupon, it is observed that atomically-dispersed $Fe-N_xC_y$ sites reach the highest ORR activity in acid media when amplified by an adequate energy binding between the metallic center and the oxygenated reaction intermediates. In contrast, $Fe@N-C$ core-shell sites reach a maximum ORR mass activity in alkaline media through a synergistic effect involving catalyst particles with metallic iron in the core and nitrogen-doped carbon in the shell.

Keywords: Fe-N-C catalyst, Co-N-C catalyst, PGM-free catalysts, alkaline exchange membrane fuel cell, proton exchange membrane fuel cell.

Introduction

The oxygen reduction reaction (ORR) electrocatalysis plays a key role in the development of sustainable and clean energy technologies, particularly when related to energy storage and conversion devices. Among these devices, fuel cells that convert the chemical energy of a fuel into electricity rely on air-reducing cathodes. Depending on the choice of electrolyte, fuel cells are operated in a broad range of pH, from acidic to neutral and alkaline conditions, as represented by the proton exchange membrane (PEMFC), microbial (MFC) and alkaline exchange membrane (AEMFC) fuel cells, respectively [1, 2]. Catalysts based on platinum (Pt) and platinum-group-metals (PGM) reach high activity and selectivity for ORR to water in acidic conditions [3], in the same way as several PGM catalysts exhibit good performances for ORR, with relative tolerance to fuel contamination, in alkaline media [4]. However, the high cost and the CO poisoning of PGM-based catalysts have been pointed out as unsolved problems for the wide-scale implementation of these devices [2, 5, 6].

Two classes of PGM-free catalysts have been widely investigated focusing on eliminating PGM for the ORR electrocatalysis: i) metal-free carbon-nitrogen (N-C) composites and ii) transition metal-incorporated carbon-nitrogen matrices (referred to as M-N-C, with M = Fe or Co) [7–9]. Recently, an extraordinary expectation towards the use of M-N-C catalysts for ORR electrocatalysis has grown, due to the recent and rapid progress in the field over the past 10 years, regarding improvement in the electrocatalytic activity, power performance, tolerance to CO and, although more challenging, improvements in stability and durability as well, observed in both high and low pH conditions [10–14]. However, a better understanding of the nature and the number of the different active sites in pyrolyzed M-N-C materials and correlations with the ORR electrocatalysis at different pH values is still required for an optimized choice of such catalysts as a function of the operating conditions, in particular regarding the operating pH of the fuel cell device.

When the pH changes from acidic (PEMFC, pH~1) to alkaline (AEMFC, pH~13) conditions, the overall four-electron O₂ reduction changes from $O_2 + 4H^+ + 4e^- \rightarrow 2H_2O$ to $O_2 + 2H_2O + 4e^- \rightarrow 4OH^-$, in acid and alkaline conditions, respectively, with implications on the mechanism, selectivity and intrinsic activity of different catalytic sites. The ORR mechanism can also proceed indirectly, first involving 2 electrons leading to H₂O₂ or HO₂⁻ peroxide intermediate, release ($O_2 + 2H^+ + 2e^- \rightarrow H_2O_2$ and $O_2 + H_2O + 2e^- \rightarrow HO_2^- + OH^-$) followed by a second sequential 2-electron transfer, whereby H₂O₂ or HO₂⁻ are reduced to H₂O or OH⁻, at

1 the same or at a different active site ($\text{H}_2\text{O}_2 + 2 \text{H}^+ + 2\text{e}^- \rightarrow 2 \text{H}_2\text{O}$ and $\text{HO}_2^- + \text{H}_2\text{O} + 2 \text{e}^- \rightarrow 3$
2 OH^-). Chemical disproportionation of H_2O_2 and HO_2^- may also be considered in both media [1,
3 15]. In addition to the different role of H^+ and OH^- species and different intermediates species
4 in the two different electrolytes, the pH difference can also modify the double layer structure,
5 resulting in different possibilities of electron-transfer mechanisms: inner- and outer-sphere [16,
6 17].
7
8
9

10
11 Many studies have investigated the nature of the different ORR active sites in M-N-C
12 catalysts [18–20], and three main types of active sites have been proposed: N_xC_y , $\text{M-N}_x\text{C}_y$ and
13 M@N-C [7], where N_xC_y sites are nitrogen functional groups in a carbon matrix, $\text{M-N}_x\text{C}_y$ are
14 atomically-dispersed nitrogen-bonded metal centers embedded in a N-doped carbon matrix and
15 M@N-C sites are a nanoparticulated metallic centers surrounded by a N-doped carbon shell
16 (itself free of $\text{M-N}_x\text{C}_y$ sites). In tuning the intrinsic ORR activity of these structurally and
17 chemically different active sites, another important parameter is the nature of the metal (M),
18 with all works reported since the 1990's pointing to iron (Fe) and cobalt (Co) as universally
19 leading to the most active PGM-free metals, regardless of the nature of the metal-based sites,
20 $\text{M-N}_x\text{C}_y$ or M@N-C [21–23].
21
22
23
24
25
26
27
28
29
30

31 Regarding Co-N-C catalysts, $\text{Co-N}_x\text{C}_y$ moieties have been pointed as the main active
32 centers that catalyze the ORR, either in alkaline or acidic conditions [24–26]. Meanwhile,
33 Co@N-C sites have shown ORR activity, with the N-C matrix providing protection of the
34 metallic core, that would otherwise be rapidly leached out in acidic medium [26]. Along the
35 same lines, the high ORR activity of Fe-N-C catalysts has been clearly linked to the content of
36 Fe- N_xC_y sites, especially in low pH conditions [7, 27]. However, it has been recently reported
37 that Fe-N-C catalysts containing Fe@N-C core-shell structures (without Fe- N_xC_y moieties) also
38 can exhibit good ORR activity, either in high or low pH conditions [19, 28, 29]. In summary, it
39 is well-established that optimized M-N-C catalysts can achieve high activities towards ORR
40 electrocatalysis, sometimes approaching those of PGM-based materials. However, it is still
41 unclear which are the truthful activities of $\text{M-N}_x\text{C}_y$ and M@N-C sites, when the catalysts are
42 used in different pH conditions.
43
44
45
46
47
48
49
50
51
52

53 Herein, we study the ORR electrocatalytic activity and mechanism of two M-N-C
54 catalysts exclusively comprising metal as $\text{M-N}_x\text{C}_y$ sites (Fe or Co), two other M-N-C catalysts
55 exclusively comprising metal as M@N-C core-shell structures (Fe or Co), and one N-C baseline
56 material synthesized similarly as the other four materials but without addition of Fe or Co
57
58
59
60
61
62
63
64
65

precursor under both acidic and alkaline conditions. The catalysts were characterized by transmission electron microscopy (TEM) and X-ray absorption spectroscopy (XAS). Their electrochemical activity was evaluated in acidic (0.1 mol L⁻¹ H₂SO₄) and alkaline (0.1 mol L⁻¹ NaOH) conditions using rotating ring-disk electrode (R(R)DE). This study demonstrates that changing the pH from acidic to alkaline results in a switch of the ability of Ar-pyrolized M-N_xC_y and M@N-C sites to reduce O₂; while M-N_xC_y sites (Fe-N_xC_y > Co-N_xC_y) are most active in acidic conditions, M@N-C (Fe@N-C > Co@N-C) reach a higher mass activity (powder mass) in alkaline conditions.

Experimental Section

Electrocatalysts synthesis

The electrocatalysts were synthesized using the method described by Zitolo *et al.* [24], in which the zinc(II) zeolitic imidazolate framework ZIF-8 (purchased from BASF, Basolite Z1200), metal(II) acetate (Fe or Co) and 1,10-phenanthroline were mixed via dry planetary ball milling in optimized ratio of 200 mg phenanthroline, 800 mg ZIF-8 and either 0.5 wt. % or 5.0 wt. % of metal (Fe or Co) to the overall mass of the three precursors. The dry mixed powder of the catalyst precursor was then heated under Ar flow with a ramp rate of 5 °C min⁻¹ to 1050 °C, and held at that temperature for 1 h, at which point the split-hinge oven was opened and the quartz tube and boat quenched to room temperature while still flowing Ar. The amount of Fe or Co before pyrolysis was either 0 (for N-C), 0.5 or 5.0 wt.% in relation to the total mass of metal salt, phenanthroline and ZIF-8. Due to about 2/3 mass loss of phenanthroline and ZIF-8 during the pyrolysis, the Fe or Co content after pyrolysis is *circa* three-times higher than in the catalyst precursor before pyrolysis. The catalysts are labeled as M_x, where M is Fe or Co and *x* is the wt. % metal in the catalyst precursor before pyrolysis, either 0.5 or 5.0. As a benchmark catalyst, Pt nanoparticles (40 wt.%) supported on graphitized carbon (TEC10EA40E) was utilized, purchased from Tanaka Kikinzoku Kogyo (TKK).

Preparation of inks and layers

Inks for the formation of PGM-free catalyst layers were prepared by dispersing the catalytic powders (10 mg) with a 5 wt.% Nafion solution (50 µL, Sigma-Aldrich), isopropanol (854 µL, Carl Roth) and ultrapure water (372 µL, Millipore, 18.2 MΩ cm), followed by ultrasonic homogenization, as described by Kumar *et al.* [30]. For the benchmark catalyst, the

1 ink was prepared in a similar way, consisting of Pt/C powder (5 mg), 5 wt.% Nafion solution
2 (54 μL), isopropanol (1446 μL) and ultrapure water (3600 μL). Then, the desired aliquot of
3 each prepared ink was dropped onto glassy carbon disc substrate of the RDE or RRDE (0.196
4 cm^2 for both), followed by drying with hot air under controlled rotation speed. The total
5 loadings were in the range of 0.1 to 0.8 mg cm^{-2} for PGM-free catalysts and 20 $\mu\text{g}_{\text{Pt/C}} \text{cm}^{-2}$ (on
6 RDE) or 10 $\mu\text{g}_{\text{Pt/C}} \text{cm}^{-2}$ (on RRDE) for the Pt/C benchmark catalyst.
7
8
9

10 11 **Electrochemical measurements**

12
13
14 Before any electrochemical experiment, the glassware, polytetrafluoroethylene (PTFE)-
15 based materials and electrodes were cleaned with a 50% v/v solution of H_2SO_4 (Merck,
16 Suprapur 96 wt.%) / H_2O_2 (Carl Roth, 30% w/w) followed by rinsing in ultrapure water (MQ
17 grade, 18.2 $\text{M}\Omega \text{ cm}$, 1–3 ppm TOC) and hot ultrapure water. All glassy carbon discs were
18 polished with 3 and 1 microns diamond polishing paste (Presi). Fresh Ar-saturated electrolytes
19 were prepared from NaOH (Alfa Aesar, 50% w/w aq. soln.), H_2SO_4 and ultrapure water to
20 obtain an electrolyte concentration of 0.1 mol L^{-1} .
21
22
23
24
25
26

27
28 The electrochemical measurements were performed using three-electrode
29 electrochemical cells with the temperature controlled at 25 $^\circ\text{C}$. A glass cell was used for acid
30 medium and PTFE cell for alkaline medium. A commercial reversible hydrogen electrode
31 (RHE, Gaskatel GmbH) coupled to the cell by Luggin capillary was used as the reference
32 electrode. To filter the high-frequency electrical noise, a Pt-wire immersed in the electrolyte
33 was connected to the reference electrode. In each electrolyte, the counter electrode was a carbon
34 sheet and the working electrode was glassy carbon coated with the investigated catalyst, with
35 loading varying depending whether RDE or RRDE measurements were performed, as described
36 below.
37
38
39
40
41
42
43
44

45 RRDE or RDE measurements were performed with Autolab PGSTAT302N and
46 PGSTAT12 potentiostat, respectively. For RDE measurements, a homemade glassy carbon
47 cylinder (glassy carbon Sigradur[®] from Hochttemperatur-Werkstoffe GmbH) embedded in a
48 PTFE cylinder, coupled to a commercial system for controlling the rotation rate (Orignalys), was
49 utilized as the working electrode. For RRDE measurements, a Pt-ring and a glassy carbon disc
50 tip (Pine Research) embedded in a PTFE rod was used.
51
52
53
54
55
56

57 For both RDE and RRDE measurements, electrochemical break-in of the thin-film
58 electrodes was performed by applying 50 cyclic voltammograms (CVs) between 0.0 and 1.0 V
59
60
61
62
63
64
65

vs. RHE at 100 mV s⁻¹ in Ar-saturated 0.1 mol L⁻¹ H₂SO₄ or 0.1 mol L⁻¹ NaOH. Then, the CVs of the thin films were recorded in the same conditions at 10 and 5 mV s⁻¹. The ORR polarization curves were recorded at 5 mV s⁻¹ in O₂-saturated electrolyte at 1600 rpm. All measurements were dynamically corrected from Ohmic drop.

The kinetic current density for ORR (i_k) was determined according to Koutecky Levich (Equation 1):

$$i_k = -\frac{(i_L \cdot i)}{(i_L - i)} \quad (1)$$

where i_L is the oxygen-diffusion limited current density at 0.2 V and i is the Faradaic current after Ohmic drop correction and capacitive current subtraction.

Consequently, the mass activity (i_{MA}) was calculated using the equation below:

$$i_{MA} = \frac{i_k}{m} \quad (2)$$

where m is the catalyst loading on the glassy carbon electrode.

For RRDE measurements, the same initial steps as described for RDE measurements were followed. Additionally, the catalyst loading was 0.1 mg cm⁻² except for the Pt catalyst for which 10 μg_{Pt} cm⁻² was utilized. To detect H₂O₂ or HO₂⁻ produced during ORR, the Pt-ring was polarized at 1.2 V vs. RHE. The peroxide quantification further requires the value of the collection efficiency (N), which was determined experimentally using the Fe³⁺/Fe²⁺ redox couple from K₃Fe(CN)₆ salt, as described before [31]. The experimental value was found to be $N = 0.24$. The equations below were utilized for determining the number of electrons transferred along the ORR (n_{e-} , Equation 3) and the peroxide percentage (Equation 4):

$$n_{e-} = \frac{4i_d}{i_d + (\frac{i_r}{N})} \quad (3)$$

$$\%H_2O_2 \text{ or } \%HO_2^- = \frac{2\frac{i_r}{N}}{(\frac{i_r}{N}) + i_d} \times 100 \quad (4)$$

where i_d and i_r are the currents at the disk and Pt-ring, respectively.

Physicochemical characterizations

1 TEM images of the electrocatalysts were recorded using a JEOL 2010 TEM instrument
2 operated at 200 kV with a point-to-point resolution of 0.19 nm. Acquisition of Co and Fe K-
3 edge X-ray absorption spectra were made at room temperature, in transmission mode at
4 SAMBA beamline of the Synchrotron SOLEIL (Gif-sur-Yvette, France), with a focusing
5 Si(220) monochromator. Pellets were prepared by mixing an adequate catalyst amount with
6 PTFE powder so as to get an optimal absorption signal. The Athena software was employed for
7 XAS data analysis, comprising the XANES (X-ray absorption near edge structure) spectra and
8 the Fourier Transforms of the EXAFS (Extended X-ray absorption fine structures) signals [32].
9
10
11
12
13
14
15
16
17

18 **Results and discussion**

19
20
21 Detailed physicochemical characterization of the catalysts using XAS, Raman and ^{57}Fe
22 Mössbauer Spectroscopy, TEM, X-EDS and XRD analyses [30, 33] have been presented in
23 previous studies published by Zitolo *et al.* [33] and Kumar *et al.* [30]. In brief, the important
24 observations previously reported are that the catalysts with 5 wt. % metal contents ($M_{5.0}$)
25 comprise metallic or metal carbide nanoparticles surrounded by a shell of N-doped graphitic
26 carbon (here referred to as M@N-C), while catalysts with low metal content ($M_{0.5}$) comprise
27 metal cations that are atomically dispersed in the N-doped carbon matrix and coordinated by
28 nitrogen atoms (here referred to as M-N_xC_y). Moreover, metal-based particles in the Fe_{5.0} and
29 Co_{5.0} catalysts were found to be exclusively Fe₃C and metallic Co, respectively. Other important
30 findings are related to the presence of more graphitic carbon structure in the neighborhood of
31 the metal-based nanoparticles for $M_{5.0}$ catalysts, as well as the presence of smaller graphite
32 crystallites in $M_{0.5}$.
33
34
35
36
37
38
39
40
41
42
43

44 Fig. 1 displays physicochemical characterizations of Fe_{0.5}, Fe_{5.0}, Co_{0.5} and Co_{5.0}. TEM
45 images shown in Fig. 1a-d evidence that the synthesized catalysts exhibit two different carbon
46 nanostructures: stacked graphitic layers (mainly for Fe_{5.0} and Co_{5.0}) and sheet-like layers with
47 poorly structured carbon, for both metals contents. This indicates that the initial highly
48 structured and organized ZIF-8 carbon and nitrogen precursor was significantly modified
49 during pyrolysis. As reported previously [26, 29], these results confirm that the catalysts present
50 particular characteristics denoting the existence of two distinct zones: i) in one case, the
51 presence of segregated metallic-based nanoparticles (10-100 nm) is seen, as confirmed by the
52 dark spots in the images of the higher metal load materials (Fe_{5.0} and Co_{5.0}) and ii) a zone
53 containing the metals atomically dispersed over the carbon-nitrogen matrix (Fe_{0.5} and Co_{0.5}).
54
55
56
57
58
59
60
61
62
63
64
65

1
2
3
4
5
6
7
8
9
10
11
12
13
14
15
16
17
18
19
20
21
22
23
24
25
26
27
28
29
30
31
32
33
34
35
36
37
38
39
40
41
42
43
44
45
46
47
48
49
50
51
52
53
54
55
56
57
58
59
60
61
62
63
64
65

Fig. 1e and 1f show XANES spectra for both types of catalysts at the Fe (energy = 7112 eV) and Co (energy = 7709 eV) K-edges, respectively, where reference spectra for Fe and Co foils and Fe₃C, were included for comparison. The high similarities between the XANES signals obtained for Fe_{5.0} and Co_{5.0} with those shown for Fe₃C and metallic Co foils, respectively, clearly indicate that the black spots in Fig. 1b and 1d for these samples are essentially zero-valent Fe and Co species [30]. In the cases of Fe_{0.5} and Co_{0.5}, the shift toward higher energy of the edge with respect to that of the metal foil and the large hump peaking at *ca.* 20 eV above the energy of the metal edge is unequivocally evidencing that the Co and Fe atoms are present in oxidized states [24, 30, 33].

Fig. 1 Physical and chemical properties of metal-N_xC_y and metal@N-C catalysts. **a-d** representative transmission electron microscopy images and **e, f** XANES and **g, h** Fourier transforms of the EXAFS spectra measured at Co or Fe K-edge. Adapted from Ref. [30] with permission from The American Chemical Society.

Fourier transforms of the EXAFS signals, either for the samples as well as for the metallic standards, are shown in Fig. 1g and 1h. First, it should be noted that the *x*-axis positions of the several peaks are related to the distance between the X-ray absorbing metal atoms and neighboring atoms present in the different coordination shells surrounding the element under investigation. However, the radial distances do not exactly correspond to the atomic distances, since a phase shift correction must be applied to precisely estimate the interatomic distance and this correction depends on the nature of the backscattering elements [33]. Here, in the case of the Fe-containing materials (Fig. 1g), the presence of the Fe-Fe coordination (peak next to 2.1-2.2 Å) is only detected for Fe_{5.0}, as concluded from comparisons with the features of the Fe₃C [34] and results reported by Zitolo *et al.* [33]. In this case, a weak shoulder is also observed at radial distance near to 1.6-1.7 Å, and this may be related to the existence of some Fe-C or Fe-N interatomic distances in the second coordination sphere, possibly assigned to Fe-C interatomic distance in Fe₃C or to Fe-C interatomic distance from a small amount of Fe-N_xC_y moieties. However, ⁵⁷Fe Mössbauer transmission spectra for the same material (catalyst named as Fe_{5.0}RP in that work) performed in our former work [30] revealed the presence of only one sextet component with Mössbauer parameters exactly matching those of Fe₃C. The ⁵⁷Fe Mössbauer spectra confirmed the conclusions drawn from XANES and EXAFS signals, and,

1 thus it may be concluded that Fe_{5.0} does not contain Fe-N bonds from Fe-N_xC_y moieties. This is
2 also in line with the absence of EXAFS signal for Fe_{5.0} at a radial distance of *ca* 1.0 Å, typical
3 for Fe-N distance in FeN_xC_y moieties. For the Fe_{0.5} material, the main peak located at 1.4 Å and
4 the less intense peak at 2.4 Å might be assigned to Fe-N and Fe-C backscatterings, respectively
5 [33]. It should be also noted that the signals for more distant shells are only clearly observed
6 for the Fe foil, indicating the absence of long-distance ordered coordination shells in Fe-
7 containing samples, particularly for Fe_{0.5}. This observation is in agreement with usual
8 propositions that, for these kind of systems, metal species are atomically dispersed in the
9 carbon-nitrogen matrix for Fe_{0.5} and, mainly as Fe₃C for Fe_{5.0}. Finally, the EXAFS of the Co-
10 based catalysts evidence two main differences with respect to the Fe-based catalysts: (i) in the
11 case of Co_{5.0}, the Co-Co coordination extends to much longer shells resembling that of the Co
12 foil, confirming that metallic Co is present as a principal species; (ii) in the case of Co_{0.5}, the
13 XANES is similar to that of Fe_{0.5} and calculations of XANES spectra for different model sites
14 showed that a good match could be obtained with either porphyrinic (CoN₄C₁₂) or defective
15 porphyrinic structures (*e.g.* CoN₃C₁₀) [24].
16
17
18
19
20
21
22
23
24
25
26
27

28 Fig. 2a and 2b show Ohmic-drop corrected CVs for all four catalysts at a fixed loading
29 in the thin-film electrode in acid and alkaline electrolytes, respectively. Results for a Fe- and
30 Co-free N-doped carbon prepared otherwise similarly (labelled M₀) are included for
31 comparison. For the M_{5.0} and M₀ catalysts and either in acid or alkaline electrolytes, the CV
32 features are those typically found for large capacitance systems, so that the currents are mostly
33 related to charge accumulation in the double layer (non-faradic and non-redox process) at the
34 catalyst | electrolyte interface. This general trend differs in the case of Fe_{0.5} in acid medium, for
35 which a redox pair, consistent with the Fe³⁺/Fe²⁺ couple, is apparent at *ca.* 0.7 V *vs.* RHE.
36 Results in Fig. 2a also show that the CV profiles exhibit similar current intensities, except for
37 the Fe_{0.5} catalyst, for which the intensities are unequivocally higher than the others, which we
38 relate to a larger carbon specific surface area [30], and/or features associated to the presence of
39 surface defects, as compared to the other cases. Another aspect is that Co_{0.5} has a larger surface
40 area than Fe_{0.5} [30], yet results in a CV that is distinct from that of Fe_{0.5} and more similar to
41 those of the other catalysts with lower BET area. This may be explained by the presence of too
42 narrow micropores in this case, which do not effectively contribute to the charge accumulation
43 in the double layer, and/or to the more organized structure of the carbon phase, leading to a
44 lower content of surface groups (N or O) and thereby decreased capacitive currents [35]. The
45 absence of redox peak assigned to Co cations in Co_{0.5} is explained by the fact that the Co²⁺/Co³⁺
46
47
48
49
50
51
52
53
54
55
56
57
58
59
60
61
62
63
64
65

1 redox in a similar Co-N-C catalyst (flash pyrolyzed) was found at potentials well above the
2 upper limit of the CVs presented here [24]. However, we noticed anodic current at high potential
3 values for Co_{5.0} in alkaline electrolyte, which indicates that Co nanoparticles are progressively
4 covered by a thin passivating layer of Co(OH)₂ followed by the oxidation of Co(OH)₂ to Co₂O₃
5 and CoOOH species, in agreement with the literature [36, 37]. Finally, the absence of Fe redox
6 features for the Fe_{5.0} catalyst in acidic conditions is consistent with previous results showing
7 that in this case all Fe is present as encapsulated metal carbide nanoparticles [30]. This implies
8 that these species, even when present in the catalyst, have no direct contact with the electrolyte.
9
10
11
12
13
14
15
16
17

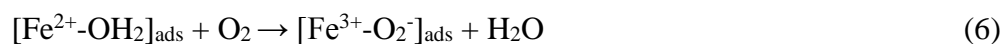
18 **Fig. 2** Electrochemical properties of Fe-N-C and Co-N-C catalysts in alkaline and acid media.
19 CVs in Ar-saturated electrolyte 0.1 mol L⁻¹ **a** H₂SO₄ and **b** NaOH at 10 mV s⁻¹; ORR
20 polarization curves in O₂-saturated electrolyte 0.1 mol L⁻¹ **c** H₂SO₄ and **d** NaOH at 5 mV s⁻¹ and
21 1600 rpm. For all measurements: 0.8 mg_{powder} cm⁻² and 25 °C. For comparison, Pt/C (20 μg_{Pt/C}
22 cm⁻²) and M₀ (N-C without Fe or Co) catalysts were utilized. Measurements were repeated at
23 least three times leading to the same results (all results and errors are tabulated in Supporting
24 Information).
25
26
27
28
29
30
31
32
33

34 Polarization curves for the ORR were constructed by subtracting the capacitive currents
35 of CV (at 5 mV s⁻¹) in Ar-saturated electrolytes from those related to the ORR, and employed
36 to evaluate the ORR activity of the catalysts (M₀, M_{0.5} and M_{5.0}). These results are shown in
37 Fig. 2c and 2d, for the acid and alkaline electrolytes, respectively, while results obtained for a
38 Pt/C catalyst were included for comparison. Generally, results show that all onset potentials are
39 higher for Fe-N-C than for Co-N-C catalysts, denoting the higher activity of Fe-N-C materials
40 for the ORR electrocatalysis. Following previous descriptors for the ORR activity on M-N-C
41 catalysts, these differences in activity can be discussed in terms of the possibility that the
42 reaction may occur involving inner- and outer-sphere electron transfer processes in alkaline
43 media [16, 17], and also in terms of the binding energy of O₂ on M²⁺ active metal species in
44 acid media [21], as detailed below.
45
46
47
48
49
50
51
52
53
54

55 In alkaline conditions, both outer- and inner-sphere electron transfer processes can co-
56 exist in the same electrocatalyst at different potentials [16, 17]. At more positive potentials (>
57 0.8 V vs. RHE), the outer-sphere electron transfer is essentially inoperant and the reaction can
58
59
60
61
62
63
64
65

occurs by the direct adsorption of desolvated O₂ on the active sites, thus following the inner-sphere electron transfer [17]. In this case, the onset potential for the ORR is dependent on the binding energy between O₂ and the active metallic center (M²⁺), which in turn is directly related to the M³⁺/M²⁺ redox potential [17, 18, 21, 38]. Based on the fact that the redox potential of Co³⁺/Co²⁺ ($E^{\circ} = 1.92$ V) is much higher than that of Fe³⁺/Fe²⁺ ($E^{\circ} = 0.77$ V) [39], the O₂ molecule adsorbs much weakly and/or to a lesser extent on Co²⁺, and in this way, the ORR onset potential for Co-N-C would be smaller than for Fe-N-C catalysts, as observed in Fig. 2d. In acidic conditions, inner-sphere electron transfer is the only possibility for the ORR electrocatalysis [16, 17]. Therefore, the causes of the differences in the ORR onset potentials on different metallic centers is explained similarly to the alkaline medium.

Fig. 2c shows that in acidic conditions, Fe_{0.5} reaches the highest onset potential among all catalysts (0.92 ± 0.01 V), being only 0.04 V smaller than that of Pt/C (see details in Supporting Information). The behavior of this catalyst confirms the high importance of having atomically dispersed Fe-N_xC_y active sites for allowing the occurrence of the Fe³⁺/Fe²⁺ oxidation process, as detected by CV. This couple seems to be the cause of the enhanced ORR electrocatalysis [40, 41] compared to the other catalysts. As already discussed in the literature [5, 17, 21], the active sites first generate Fe²⁺ from the reduction of Fe³⁺ (Equation 5), which next promotes the displacement of adsorbed H₂O by O₂, accompanied by an electron transfer of Fe²⁺ to O₂ (Equation 6); the [Fe³⁺-OH]⁻_{ads} species would be regenerated in the following reaction step, so that the process becomes cyclically repeated:



In acid media, other studies have shown that the onset potential for the ORR is directly related to the redox potential of the metal in the M-N_xC_y sites [17, 21, 28]. Here, such a redox process was only evident for Fe_{0.5}; it was not seen for Fe_{5.0} because in this case the only catalyst metal phase is formed by Fe₃C particles surrounded by a nitrogen-carbon shell (Fe@N-C). Finally, in the case of the Co-N-C catalysts in acid media, although results in Fig. 1 show that Co_{0.5} presents the same atomic distribution as Fe_{0.5}, the corresponding CV does not evidence the occurrence of redox processes. This is because the presence of redox features of Co only appears at potentials well above the onset of the ORR, as is the case of Co³⁺/Co²⁺. From the results in Fig. 2c, it is seen that the activity of the Co-N-C catalysts for the ORR is in fact not

1
2 so much superior to that of M_0 , which demonstrates the smaller role of $Co-N_xC_y$ and $Co@N-C$
3 for the promotion of the ORR electrocatalysis.

4
5 In alkaline medium, for the Fe-N-C catalysts (Fig. 2d), results show that the ORR onset
6 potentials are very close (or equal, in the case of $Fe_{5.0}$) to that of Pt/C (0.97 ± 0.01 V), that is,
7 0.97 ± 0.01 V for $Fe_{5.0}$ and 0.95 ± 0.01 V for $Fe_{0.5}$. This high catalytic activity of $Fe_{5.0}$ evidences
8 that in this medium, the Fe@N-C sites are active for the ORR, in contrast to the acid medium.
9 Although substantially smaller than those of the Fe-N-C materials, the same catalytic
10 phenomena are seen for the $Co@N-C$ and $Co-N_xC_y$ materials, for which the values of onset
11 potential are 0.84 ± 0.01 V and 0.82 ± 0.01 V, respectively. In fact, a similar enhancement of
12 catalytic activity is also seen in the absence of metallic centers (M_0). The higher activity of the
13 Fe@N-C active sites in alkaline medium can be assigned to the enhancement of electrical
14 conductivity of nitrogen-carbon and a synergistic effect between the metallic centers and the
15 nitrogen-carbon shell. This is in line with recent results demonstrating that a higher degree of
16 graphitization of carbon is beneficial to the electrical conductivity [42], and that synergies
17 between the nitrogen-carbon shell and metallic centers contribute to efficient ORR
18 electrocatalysis [19, 28, 43–46].

19
20 Another aspect to be discussed is the cause of the positive shift on the onset potential
21 when the pH is changed from low to high values. This fact may be related to the OH_{ads} coverage
22 and its desorption to regenerate the active metallic center M^{2+} [5, 18, 21]. Thus, a higher
23 concentration of OH^- species in the electrolyte (alkaline media) seems to favor high coverages
24 of OH_{ads} . In contrast, the effective OH_{ads} coverage in acidic conditions requires more energy
25 due to the much smaller OH^- availability to generate and regenerate the M^{2+} active center, as
26 shown above (Equations 5-6); also Fe^{3+} species can be poisoned by strong adsorption of H_2O ,
27 blocking the generation of Fe^{2+} species active for ORR [47].

28
29 Interestingly, the change in pH from acid to alkaline leads to a lower increase of the
30 onset (half-wave) potentials by 30 mV (30 mV) for $Fe_{0.5}$ and 100 mV (70 mV) for $Fe_{5.0}$. This
31 indicates that the activity of the Fe- N_xC_y sites in the present case is little affected by the pH, so
32 that the $Fe_{0.5}$ catalyst can promote the ORR electrocatalysis with similar efficiency, either at
33 high or low H^+/OH^- concentrations. In contrast, results for Fe@N-C sites denote larger
34 variations of onset/half-wave potentials, but the shift is smaller in the case of the half-wave
35 potential, possibly indicating some occurrence of inner- and outer-sphere electron transfer
36
37
38
39
40
41
42
43
44
45
46
47
48
49
50
51
52
53
54
55
56
57
58
59
60
61
62
63
64
65

1 mechanisms in alkaline medium, depending on the electrode potential. These behaviors were
2 not found in Co-N-C catalysts, and, then this feature is exclusively related to Fe-N-C catalysts.
3

4 For the investigation of PGM-free catalyst loading effects on the mass activity for ORR
5 electrocatalysis was selected the Fe_{0.5} catalyst in both pH conditions. Then, that catalyst loading
6 effect was evaluated for Fe_{0.5} in the range of 0.1 to 0.8 mg_{powder} cm⁻² in 0.1 mol L⁻¹ H₂SO₄ and
7 0.1 mol L⁻¹ NaOH electrolytes, and the results are shown in Fig. 3. CV profiles in Fig. 3a and
8 3b exhibit the expected proportional increase of the capacitive currents from low to high catalyst
9 loadings in both pH conditions. For example, at 0.4 V, the capacitive currents increase linearly
10 with the catalyst loading (see Fig. 1 – Supporting Information). This is mainly caused by the
11 increase in the electrochemically available area, which is more pronounced in acidic conditions
12 due to some contributions of currents related to redox processes of Fe³⁺/Fe²⁺ and of oxygen
13 functional groups present in the carbon matrix. As described in the literature [48], the oxidative
14 process of carbon causes changes in the magnitude of the capacitive current at low pHs, while
15 in alkaline media the graphitic structures are less functionalized because they become
16 hydrophilic enough for releasing some carbon functional groups.
17
18
19
20
21
22
23
24
25
26
27
28
29
30

31 **Fig. 3** Electrochemical properties of different Fe_{0.5} catalyst loadings. CVs in Ar-saturated
32 electrolyte 0.1 mol L⁻¹ **a** H₂SO₄ and **b** NaOH at 10 mV s⁻¹; ORR polarization curves in O₂-
33 saturated electrolyte 0.1 mol L⁻¹ **c** H₂SO₄ and **d** NaOH at 5 mV s⁻¹ and 1600 rpm. All
34 measurements were performed at 25 °C. Measurements were repeated at least three times
35 leading to the same results (all results and errors are tabulated in Supporting Information).
36
37
38
39
40
41

42 In Fig. 3c and 3d, the results evidence a displacement of the ORR onset and half-wave
43 potentials to higher values and increased oxygen diffusion limited current densities (in the range
44 of 0.0 V to 0.55 V) with the increase of the catalyst loading, with the effects being higher in the
45 acid medium. This increase in the oxygen diffusion limited current densities with the increase
46 of the catalyst loading is probably related to the increased residence time of
47 reactant/intermediate species [49, 50], like OH⁻, O₂, H₂O₂ or HO₂⁻ inside the catalyst layer,
48 enhancing their further reduction to complete the 4-electron process. Moreover, a sufficient
49 number of active sites is necessary to catalyze the ORR efficiently [49, 50], otherwise no
50 oxygen diffusion limited currents appear, which in acid media, seems to be the case for loadings
51 ≤ 0.2 mg_{powder} cm⁻². In alkaline electrolytes, this effect may be minimized by the electrostatic
52
53
54
55
56
57
58
59
60
61
62
63
64
65

1 interaction of anionic HO_2^- species with the Fe^{2+} cation from $\text{Fe-N}_x\text{C}_y$ active sites [16, 17, 40],
2 thus driving the ORR to OH^- even in thin catalyst layers (as also observed in Fig. 4) [51].
3
4
5
6

7 **Fig. 4** RRDE measurements of Fe-N-C and Co-N-C catalysts. Peroxide percentage produced
8 from ORR electrocatalysis in O_2 -saturated electrolyte 0.1 mol L^{-1} **a** H_2SO_4 and **b** NaOH at 5
9 mV s^{-1} and 1600 rpm. For all measurements: $0.1 \text{ mg}_{\text{powder}} \text{ cm}^{-2}$ and $25 \text{ }^\circ\text{C}$. For comparison, Pt/C
10 ($10 \text{ } \mu\text{g}_{\text{Pt/C}} \text{ cm}^{-2}$) and M_0 (without Fe or Co) catalysts were utilized (all results are tabulated in
11 Supporting Information).
12
13
14
15

16
17
18
19
20 The oxygen diffusion limited currents for the M-N-C catalysts are all smaller than that
21 observed for Pt/C (Fig. 2c and 2d), that is known to lead to a predominant 4-electron ORR
22 mechanism (O_2 is mostly reduced to H_2O in acid or OH^- in alkaline electrolytes). To discuss
23 these issues, the percentages of $\text{H}_2\text{O}_2/\text{HO}_2^-$ formation and the number of electrons involved in
24 the ORR were obtained from rotating ring-disk measurements and these results are shown in
25 Fig. 4. Generally speaking, the n_{e^-} values for the M-N-C catalysts, and more specifically Fe-N-
26 C, are not so different from that of Pt/C, either in acid or alkaline media, but this is more evident
27 in the alkaline medium (see Tables 1-2 – Supporting Information). Results related to the
28 $\text{H}_2\text{O}_2/\text{HO}_2^-$ formation are consistent with the above observations related to the number of
29 transferred electrons in the ORR, as would be expected because the same data and principles
30 are used in the calculations of n_{e^-} and $\% \text{H}_2\text{O}_2/\text{HO}_2^-$. These aspects regarding the number of
31 electrons/percentages of $\text{H}_2\text{O}_2/\text{HO}_2^-$ formation confirm that in the alkaline medium $\text{Fe-N}_x\text{C}_y$
32 and Fe@N-C sites perform the reaction involving similar pathways and provide additional
33 evidence that the Fe@N-C sites stabilize the HO_2^- intermediate as efficiently as $\text{Fe-N}_x\text{C}_y$.
34 Therefore, synergistic effects in the Fe@N-C catalyst can provide an adequate energy binding
35 between HO_2^- and the nitrogen-carbon shell, even without the direct contact between the Fe
36 metallic center and the reactants or intermediates. In the cases of the Co-N-C materials, inferior
37 n_{e^-} values regularly ranging from 3 to 2 are observed in Fig. 4 and Tables 1-2 (Supporting
38 Information).
39
40
41
42
43
44
45
46
47
48
49
50
51
52
53
54
55

56 Adequate adsorption energies of oxygenated intermediates species has been pointed to
57 be essential for achieving high n_{e^-} values in the ORR, and in this sense the anionic HO_2^- species
58 formed along the ORR in alkaline conditions seems to be more strongly bound to the catalyst
59
60
61
62
63
64
65

1 compared to the H_2O_2 species in acidic media, ensuring larger occurrence of the complete ORR
2 electrocatalysis to OH^- . However, the higher amounts of $\text{H}_2\text{O}_2/\text{HO}_2^-$ detected by the ring for the
3 Co-catalysts, compared to the Fe-catalysts, may mean that the binding energies of $\text{H}_2\text{O}_2/\text{HO}_2^-$
4 on Co- N_xC_y sites are small [21, 24, 52], as it would be also expected for the Co@N-C sites. In
5 fact, trends observed here regarding the onset potentials, oxygen diffusion-limited currents, and
6 number of electrons transferred in the ORR were similar to those observed in other studies of
7 the ORR electrocatalysis in other Fe-N-C and Co-N-C catalysts [24, 53–55].
8
9

10
11
12
13 Further information about the reaction mechanism was obtained from Tafel plots
14 constructed in the high-potential region of the ORR polarization curves and expressed in terms
15 of the mass activity of the catalysts (i_{MA}), calculated as described in the experimental section.
16 Results are shown in Fig. 5. The slopes of the resulting lines (Tafel slopes) were calculated, and
17 the values are summarized in Table S1 and Table S2 (see Supporting Information). First, it is
18 noted that $\text{Fe}_{0.5}$ and $\text{Fe}_{5.0}$ exhibit higher Tafel slopes as compared to $\text{Co}_{0.5}$ and $\text{Co}_{5.0}$ in both
19 media (Fig. 5a and 5b), and this is consistent with the occurrence of distinct ORR mechanisms
20 and/or rate-determining steps in the two class of investigated materials. This observation is
21 similar to those reported in published works when comparing Fe- vs. Co-based catalysts [22,
22 24, 53, 56].
23
24
25
26
27
28
29
30
31

32
33 The Tafel slopes for $\text{Fe}_{0.5}$ and $\text{Fe}_{5.0}$ catalysts are essentially the same in acid or alkaline
34 media, demonstrating that the rate determining step of the ORR mechanism may be the same
35 in both cases, although involving different active sites and for $\text{Fe}_{0.5}$ in acid medium
36 corresponding to a direct redox-mediated process. This implies that the different ORR activities
37 seen for $\text{Fe}_{0.5}$ and $\text{Fe}_{5.0}$ in acid media (as evidenced for the different reaction overpotentials at a
38 given mass activity) may be related to the different catalyst specific active areas and/or different
39 synergistic phenomena related to the different nature of the active centers. In alkaline media,
40 since no redox features are detected but the activities are also close, one may conclude that the
41 rate determining step, the ORR mechanism and eventually the specific active area are very
42 similar for both catalysts. Finally, the results evidence the absence of mass-transport and
43 conductivity problems related to the thickness/structure of catalytic layers, so that the
44 magnitude of Tafel slopes is only related to the ORR mechanism [57].
45
46
47
48
49
50
51
52
53
54
55
56
57

58 **Fig. 5** Mass-transport-corrected Tafel plots of Fe-N-C and Co-N-C catalysts at fixed loading,
59 and for $\text{Fe}_{0.5}$ on different catalyst loadings. Performed in O_2 -saturated electrolyte 0.1 mol L^{-1} **a**,
60
61
62
63
64
65

1 **c** H₂SO₄ and **b, d** NaOH at 5 mV s⁻¹, 1600 rpm and 25 °C. For **a, b** measurements: 0.8 mg_{powder}
2 cm⁻², Pt/C (10 μg_{Pt/C} cm⁻²) and M₀ (without Fe or Co) catalysts were utilized. Measurements
3 were repeated at least three times leading to the same results (all results and errors are tabulated
4 in Supporting Information). In **c, d** panels, different Fe_{0.5} loadings were used.
5
6
7
8
9

10 For easier comparisons of the mass activity towards the ORR of materials, the
11 previously calculated values at 0.85 V were plotted for each set of catalyst in both
12 electrolytes (Fig. 6). Analyzing the results in acidic conditions (Fig. 6a), it is concluded that
13 among all M-N-C catalysts, Fe_{0.5} presents the highest mass activity for the ORR, followed by
14 Fe_{5.0}, Co_{0.5} and Co_{5.0}, as shown in Fig. 5a and 6a. This superior activity of Fe_{0.5} compared to
15 that of Fe_{5.0} indicates a superior activity of Fe-N_xC_y sites compared to Fe@N-C; this trend is
16 maintained for Co_{0.5} with respect to Co_{5.0}. Therefore, we conclude that M-N_xC_y sites provide
17 higher mass activity than M@N-C in acid conditions.
18
19
20
21
22
23
24
25
26
27
28

29 **Fig. 6** Mass activity towards the ORR (*i*_{MA}) measured at 0.85 V for **a** all catalysts investigated
30 in this study and **b** for different Fe_{0.5} catalyst loadings. All ORR experiments conducted at 1600
31 rpm, 5 mV s⁻¹, 25 °C in O₂-saturated 0.1 mol L⁻¹ (**red**) H₂SO₄ or (**blue**) NaOH electrolytes.
32 Catalyst loadings of 0.8 mg_{powder} cm⁻² were employed in **a**. Measurements were repeated at least
33 three times leading to the same results (all results and errors are tabulated in Supporting
34 Information).
35
36
37
38
39
40
41
42
43

44 In alkaline solution, results show that Fe_{5.0} presents the highest mass activity for the
45 ORR, followed by Fe_{0.5}, Co_{5.0}, and Co_{0.5}. Therefore, generally speaking, it is seen that a high
46 number of M@N-C sites (present in the catalysts with high metal content) can provide higher
47 mass activity in alkaline medium as compared to a low number of M-N_xC_y sites, that is
48 predominant in catalysts with low metal content. These results show that, in alkaline media, the
49 presence of atomically-dispersed M-N_xC_y sites is not mandatory for the promotion of the ORR
50 electrocatalysis with good efficiency. However, this mass activity distinction for materials
51 containing M@N-C and M-N_xC_y sites seems to be evident only for Ar-pyrolyzed catalysts (or
52 another inert gas). Indeed, recently, Santori *et al.*[58] have shown that other factors can lead to
53 increased mass activity when switching from Ar- to NH₃-treated catalysts containing
54
55
56
57
58
59
60
61
62
63
64
65

1
2
3
4
5
6
7
8
9
10
11
12
13
14
atomically-dispersed Fe-N_xC_y sites. Further, another important aspect is that the catalyst without a metallic center (M₀) resulted in the poorest mass activity towards the ORR, stressing the crucial importance of having the metallic M@N-C or M-N_xC_y active sites for catalyzing the ORR, particularly in the case of iron. This is in agreement with the observation above reported, confirming that synergistic effects between the M²⁺ active metallic center and nitrogen-carbon shell (M@N-C) enhance the ORR mass activity, more than M-N_xC_y sites in high OH⁻ concentrations. Previous experimental studies provide support for the high activities found for Fe@N-C sites in alkaline media [10, 28, 44, 46, 59–61].

15
16
17
18
19
20
21
22
23
24
25
26
27
28
29
30
31
32
33
34
35
36
37
38
39
40
41
42
43
44
45
46
47
48
49
50
51
52
53
54
55
56
57
58
59
60
61
62
63
64
65
Fig. 6b allows discussing the mass activity as a function of the Fe_{0.5} catalyst loading for the two pH conditions. It is first noted that the mass activities are higher in alkaline than in acid media (except for 0.8 mg_{powder} cm⁻²), following the same trends found in Fig. 6a. Also, it is noted that there is an increase of the ORR mass activity with increased catalyst loading in acidic conditions, while the opposite occurs in alkaline media. These results confirm the need of longer residence time of reactants and/or intermediates inside the catalyst layer, as well as of the amount of Fe-N_xC_y sites in acid medium, while this is not the case in alkaline medium. These results have strong implications for the design of PGM-free catalysts layers in the cathodes of PEMFC and AEMFC.

66 67 68 69 70 71 72 73 74 75 76 77 78 79 80 81 82 83 84 85 86 87 88 89 90 91 92 93 94 95 96 97 98 99 100 **Conclusions**

101
102
103
104
105
106
107
108
109
110
111
112
113
114
115
116
117
118
119
120
121
122
123
124
125
126
127
128
129
130
131
132
133
134
135
136
137
138
139
140
141
142
143
144
145
146
147
148
149
150
151
152
153
154
155
156
157
158
159
160
161
162
163
164
165
166
167
168
169
170
171
172
173
174
175
176
177
178
179
180
181
182
183
184
185
186
187
188
189
190
191
192
193
194
195
196
197
198
199
200
201
202
203
204
205
206
207
208
209
210
211
212
213
214
215
216
217
218
219
220
221
222
223
224
225
226
227
228
229
230
231
232
233
234
235
236
237
238
239
240
241
242
243
244
245
246
247
248
249
250
251
252
253
254
255
256
257
258
259
260
261
262
263
264
265
266
267
268
269
270
271
272
273
274
275
276
277
278
279
280
281
282
283
284
285
286
287
288
289
290
291
292
293
294
295
296
297
298
299
300
301
302
303
304
305
306
307
308
309
310
311
312
313
314
315
316
317
318
319
320
321
322
323
324
325
326
327
328
329
330
331
332
333
334
335
336
337
338
339
340
341
342
343
344
345
346
347
348
349
350
351
352
353
354
355
356
357
358
359
360
361
362
363
364
365
366
367
368
369
370
371
372
373
374
375
376
377
378
379
380
381
382
383
384
385
386
387
388
389
390
391
392
393
394
395
396
397
398
399
400
401
402
403
404
405
406
407
408
409
410
411
412
413
414
415
416
417
418
419
420
421
422
423
424
425
426
427
428
429
430
431
432
433
434
435
436
437
438
439
440
441
442
443
444
445
446
447
448
449
450
451
452
453
454
455
456
457
458
459
460
461
462
463
464
465
466
467
468
469
470
471
472
473
474
475
476
477
478
479
480
481
482
483
484
485
486
487
488
489
490
491
492
493
494
495
496
497
498
499
500
501
502
503
504
505
506
507
508
509
510
511
512
513
514
515
516
517
518
519
520
521
522
523
524
525
526
527
528
529
530
531
532
533
534
535
536
537
538
539
540
541
542
543
544
545
546
547
548
549
550
551
552
553
554
555
556
557
558
559
560
561
562
563
564
565
566
567
568
569
570
571
572
573
574
575
576
577
578
579
580
581
582
583
584
585
586
587
588
589
590
591
592
593
594
595
596
597
598
599
600
601
602
603
604
605
606
607
608
609
610
611
612
613
614
615
616
617
618
619
620
621
622
623
624
625
626
627
628
629
630
631
632
633
634
635
636
637
638
639
640
641
642
643
644
645
646
647
648
649
650
651
652
653
654
655
656
657
658
659
660
661
662
663
664
665
666
667
668
669
670
671
672
673
674
675
676
677
678
679
680
681
682
683
684
685
686
687
688
689
690
691
692
693
694
695
696
697
698
699
700
701
702
703
704
705
706
707
708
709
710
711
712
713
714
715
716
717
718
719
720
721
722
723
724
725
726
727
728
729
730
731
732
733
734
735
736
737
738
739
740
741
742
743
744
745
746
747
748
749
750
751
752
753
754
755
756
757
758
759
760
761
762
763
764
765
766
767
768
769
770
771
772
773
774
775
776
777
778
779
780
781
782
783
784
785
786
787
788
789
790
791
792
793
794
795
796
797
798
799
800
801
802
803
804
805
806
807
808
809
810
811
812
813
814
815
816
817
818
819
820
821
822
823
824
825
826
827
828
829
830
831
832
833
834
835
836
837
838
839
840
841
842
843
844
845
846
847
848
849
850
851
852
853
854
855
856
857
858
859
860
861
862
863
864
865
866
867
868
869
870
871
872
873
874
875
876
877
878
879
880
881
882
883
884
885
886
887
888
889
890
891
892
893
894
895
896
897
898
899
900
901
902
903
904
905
906
907
908
909
910
911
912
913
914
915
916
917
918
919
920
921
922
923
924
925
926
927
928
929
930
931
932
933
934
935
936
937
938
939
940
941
942
943
944
945
946
947
948
949
950
951
952
953
954
955
956
957
958
959
960
961
962
963
964
965
966
967
968
969
970
971
972
973
974
975
976
977
978
979
980
981
982
983
984
985
986
987
988
989
990
991
992
993
994
995
996
997
998
999
1000

1
2
3
4
5
6
7
8
9
10
11
12
13
14
15
16
17
18
19
20
21
22
23
24
25
26
27
28
29
30
31
32
33
34
35
36
37
38
39
40
41
42
43
44
45
46
47
48
49
50
51
52
53
54
55
56
57
58
59
60
61
62
63
64
65

metallic center with surface hydroxyl and other intermediates drives the ORR electrocatalysis more effectively. Finally, Fe@N-C stabilizes HO₂⁻ intermediates adequately resulting in predominance of 4-electron transfer per oxygen molecule.

Acknowledgments

The authors thank the French National Research Agency through the CAT2CAT and ANIMA projects (Grant No. ANR-16-CE05-0007-03), the Coordenação de Aperfeiçoamento de Pessoal de Nível Superior (CAPES), Brazil (process number: 1614344), CAPES/COFECUB program (process numbers: 88887-187755/2018-00 and Ph-C 914/18) and the São Paulo State Research Foundation (FAPESP – process number: 2013/16930-7) for financial supports. The Synchrotron SOLEIL (Gif-sur Yvette, France) is acknowledged for provision of synchrotron radiation facilities at beamline SAMBA (Proposal No. 20171318). We also acknowledge Qingying Jia (Northeastern University, Boston, USA) for providing the EXAFS spectrum of Fe₃C.

References

1. Shao M, Chang Q, Dodelet J-P, Chenitz R (2016) Recent advances in electrocatalysts for oxygen reduction reaction. *Chem Rev* 116:3594–3657.
2. Lopes T, Kucernak A, Malko D, Ticianelli EA (2016) Mechanistic insights into the oxygen reduction reaction on Metal–N–C electrocatalysts under fuel cell conditions. *ChemElectroChem* 3:1580–1590.
3. Gasteiger HA, Kocha SS, Sompalli B, Wagner FT (2005) Activity benchmarks and requirements for Pt, Pt-alloy, and non-Pt oxygen reduction catalysts for PEMFCs. *Appl Catal B Environ* 56:9–35.
4. Serov A, Zenyuk I V., Arges CG, Chatenet M (2018) Hot topics in alkaline exchange membrane fuel cells. *J Power Sources* 375:149–157.
5. Li J, Alsudairi A, Ma ZF, et al (2017) Asymmetric volcano trend in oxygen reduction activity of Pt and non-Pt catalysts: In situ identification of the site-blocking effect. *J Am Chem Soc* 139:1384–1387.

- 1
2
3
4
5
6
7
8
9
10
11
12
13
14
15
16
17
18
19
20
21
22
23
24
25
26
27
28
29
30
31
32
33
34
35
36
37
38
39
40
41
42
43
44
45
46
47
48
49
50
51
52
53
54
55
56
57
58
59
60
61
62
63
64
65
6. Strateg Anal Inc. Mass Production Cost Estimation of Direct H₂ PEM Fuel Cell Systems for Transportation Applications : 2013 Update (2013) US Department of Energy, Washington.
https://www.energy.gov/sites/prod/files/2014/11/f19/fcto_sa_2013_pemfc_transportation_cost_analysis.pdf . Accessed 24 May 2019.
7. Li J, Ghoshal S, Liang W, et al (2016) Structural and mechanistic basis for the high activity of Fe-N-C catalysts toward oxygen reduction. *Energy Environ Sci* 9:2418–2432.
8. do Rêgo UA, Lopes T, Bott-Neto JL, et al (2019) Non-noble Fe-N_x/C electrocatalysts on tungsten carbides/N-doped carbons for the oxygen reduction reaction. *Electrocatalysis* 10:134–148.
9. do Rêgo UA, Lopes T, Bott-Neto JL, et al (2018) Oxygen reduction electrocatalysis on transition metal-nitrogen modified tungsten carbide nanomaterials. *J Electroanal Chem* 810:222–231.
10. Zhong G, Wang H, Yu H, Peng F (2015) Nitrogen doped carbon nanotubes with encapsulated ferric carbide as excellent electrocatalyst for oxygen reduction reaction in acid and alkaline media. *J Power Sources* 286:495–503.
11. Brocato S, Serov A, Atanassov P (2013) pH dependence of catalytic activity for ORR of the non-PGM catalyst derived from heat-treated Fe-phenanthroline. *Electrochim Acta* 87:361–365.
12. Meng H, Jaouen F, Proietti E, et al (2009) pH-effect on oxygen reduction activity of Fe-based electro-catalysts. *Electrochem Commun* 11:1986–1989.
13. Elumeeva K, Ren J, Antonietti M, Feller TP (2015) High surface iron/cobalt-containing nitrogen-doped carbon aerogels as non-precious advanced electrocatalysts for oxygen reduction. *ChemElectroChem* 2:584–591.
14. Rojas-Carbonell S, Artyushkova K, Serov A, et al (2018) Effect of pH on the activity of platinum group metal-free catalysts in oxygen reduction reaction. *ACS Catal* 8:3041–3053.
15. Ge X, Sumboja A, Wu D, et al (2015) Oxygen reduction in alkaline media: From mechanisms to recent advances of catalysts. *ACS Catal* 5:4643–4667.

16. Ramaswamy N, Mukerjee S (2011) Influence of inner- and outer-sphere electron transfer mechanisms during electrocatalysis of oxygen reduction in alkaline media. *J Phys Chem C* 115:18015–18026.
17. Ramaswamy N, Tylus U, Jia Q, Mukerjee S (2013) Activity descriptor identification for oxygen reduction on nonprecious electrocatalysts: Linking surface science to coordination chemistry. *J Am Chem Soc* 135:15443–15449.
18. Jia Q, Ramaswamy N, Hafiz H, et al (2015) Experimental observation of redox-induced Fe-N switching behavior as a determinant role for oxygen reduction activity. *ACS Nano* 9:12496–12505.
19. Zhong L, Frandsen C, Mørup S, et al (2018) ⁵⁷Fe-Mössbauer spectroscopy and electrochemical activities of graphitic layer encapsulated iron electrocatalysts for the oxygen reduction reaction. *Appl Catal B Environ* 221:406–412.
20. Singh SK, Takeyasu K, Nakamura J (2018) Active sites and mechanism of oxygen reduction reaction electrocatalysis on nitrogen-doped carbon materials. *Adv Mater* 1804297:1–17.
21. Zagal JH, Koper MTM (2016) Reactivity descriptors for the activity of molecular MN₄ catalysts for the oxygen reduction reaction. *Angew Chemie - Int Ed* 55:14510–14521.
22. Wu G, More KL, Johnston CM, Zelenay P (2011) High-performance electrocatalysts for oxygen reduction derived from polyaniline, iron, and cobalt. *Science* (80) 332:443–447.
23. Chen, Z.; Dodelet, J. P.; Zhang J (eds) (2014) *Non-noble metal fuel cell catalysts*. Wiley, New York.
24. Ranjbar-Sahraie N, Zitolo A, Fonda E, et al (2017) Identification of catalytic sites in cobalt-nitrogen-carbon materials for the oxygen reduction reaction. *Nat Commun* 8:1–10.
25. Subramanian P, Mohan R, Schechter A (2017) Unraveling the oxygen-reduction sites in graphitic-carbon Co–N–C-type electrocatalysts prepared by single-precursor pyrolysis. *ChemCatChem* 9:1969–1978.
26. Perkas N, Schechter A, Gedanken A, et al (2017) Electrochemical oxygen reduction activity of metal embedded nitrogen doped carbon nanostructures derived from pyrolysis

of nitrogen-rich guanidinium salt. *J Electrochem Soc* 164:F781–F789.

27. Dodelet JP, Chenitz R, Yang L, Lefèvre M (2014) A new catalytic site for the electroreduction of oxygen? *ChemCatChem* 6:1866–1867.
28. Strickland K, Miner E, Jia Q, et al (2015) Highly active oxygen reduction non-platinum group metal electrocatalyst without direct metal-nitrogen coordination. *Nat Commun* 6:1–8.
29. Varnell JA, Tse ECM, Schulz CE, et al (2016) Identification of carbon-encapsulated iron nanoparticles as active species in non-precious metal oxygen reduction catalysts. *Nat Commun* 7:1–9.
30. Kumar K, Gairola P, Ranjbar-Sahraie N, Maillard F, et al (2018) Physical and chemical considerations for improving catalytic activity and stability of non-precious-metal oxygen reduction reaction catalysts. *ACS Catal* 8:11264–11276.
31. Paulus UA, Schmidt TJ, Gasteiger HA, Behm RJ (2001) Oxygen reduction on a high-surface area Pt/Vulcan carbon catalyst: A thin-film rotating ring-disk electrode study. *J Electroanal Chem* 495:134–145.
32. Ravel B, Newville M (2005) ATHENA, ARTEMIS, HEPHAESTUS: Data analysis for X-ray absorption spectroscopy using IFEFFIT. *J Synchrotron Radiat* 12:537–541.
33. Zitolo A, Goellner V, Armel V, et al (2015) Identification of catalytic sites for oxygen reduction in iron- and nitrogen-doped graphene materials. *Nat Mater* 14:937–942.
34. Yuan K, Sfaelou S, Qiu M, et al (2018) Synergetic contribution of boron and Fe-N_x species in porous carbons toward efficient electrocatalysts for oxygen reduction reaction. *ACS Energy Lett* 3:252–260.
35. Raymundo-Piñero E, Kierzek K, Machnikowski J, Béguin F (2006) Relationship between the nanoporous texture of activated carbons and their capacitance properties in different electrolytes. *Carbon* 44:2498–2507.
36. Cowling RD, Riddiford AC (1969) The anodic behaviour of cobalt in alkaline solutions. *Electrochim Acta* 14:981–989.
37. Favaro M, Yang J, Nappini S, et al (2017) Understanding the oxygen evolution reaction

Mmechanism on CoO_x using *operando* ambient-pressure X-ray photoelectron spectroscopy. *J Am Chem Soc* 139:8960–8970.

38. Zúñiga C, Candia-Onfray C, Venegas R, et al (2019) Elucidating the mechanism of the oxygen reduction reaction for pyrolyzed Fe-N-C catalysts in basic media. *Electrochem commun.* 102:78-82.
39. Bard AJ, Faulkner LR (2001) *Electrochemical methods: fundamentals and applications.* Wiley, New York.
40. Ramaswamy N, Mukerjee S (2012) Fundamental mechanistic understanding of zlectrocatalysis of oxygen reduction on Pt and Non-Pt surfaces: Acid versus alkaline media. *Adv Phys Chem* 2012:1–17.
41. Tylus U, Jia Q, Strickland K, et al (2014) Elucidating oxygen reduction active sites in pyrolyzed metal-nitrogen coordinated non-precious-metal electrocatalyst systems. *J Phys Chem C* 118:8999–9008.
42. Pérez-Rodríguez S, Torres D, Lázaro MJ (2018) Effect of oxygen and structural properties on the electrical conductivity of powders of nanostructured carbon materials. *Powder Technol* 340:380–388.
43. Deng D, Yu L, Chen X, et al (2013) Iron encapsulated within pod-like carbon nanotubes for oxygen reduction reaction. *Angew Chemie - Int Ed* 52:371–375.
44. Zhu J, Xiao M, Liu C, et al (2015) Growth mechanism and active site probing of $\text{Fe}_3\text{C}@N$ -doped carbon nanotubes/C catalysts: guidance for building highly efficient oxygen reduction electrocatalysts. *J Mater Chem A* 3:21451–21459.
45. Watanabe M (1991) Design of alloy electrocatalysts for CO_2 reduction. *J Electrochem Soc* 138:3382.
46. Hu Y, Jensen JO, Zhang W, et al (2014) Hollow spheres of iron carbide nanoparticles encased in graphitic layers as oxygen reduction catalysts. *Angew Chemie - Int Ed* 53:3675–3679.
47. Anderson AB, Sidik RA (2004) Oxygen electroreduction on Fe^{II} and Fe^{III} coordinated to N_4 chelates. Reversible potentials for the intermediate steps from quantum theory . *J Phys Chem B* 108:5031–5035.

- 1
2
3
4
5
6
7
8
9
10
11
12
13
14
15
16
17
18
19
20
21
22
23
24
25
26
27
28
29
30
31
32
33
34
35
36
37
38
39
40
41
42
43
44
45
46
47
48
49
50
51
52
53
54
55
56
57
58
59
60
61
62
63
64
65
48. Yi Y, Weinberg G, Prenzel M, et al (2017) Electrochemical corrosion of a glassy carbon electrode. *Catal Today* 295:32–40.
 49. Freitas KS, Concha BM, Ticianelli EA, Chatenet M (2011) Mass transport effects in the borohydride oxidation reaction - Influence of the residence time on the reaction onset and faradaic efficiency. *Catal Today* 170:110–119.
 50. A. Schneider, L. Colmenares, Y. E. Seidel, Z. Jusys, B. Wickman BK and RJB (2008) Transport effects in the oxygen reduction reaction on nanostructured, planar glassy carbon supported Pt/GC model electrodes. *Phys Chem Chem Phys* 10:1931–1943.
 51. Serov A, Artyushkova K, Andersen NI, et al (2015) Original mechanochemical synthesis of non-platinum group metals oxygen reduction reaction catalysts assisted by sacrificial support method. *Electrochim Acta* 179:154–160.
 52. Goellner V, Armel V, Zitolo A, et al (2015) Degradation by hydrogen peroxide of metal-nitrogen-carbon catalysts for oxygen reduction. *J Electrochem Soc* 162:H403–H414.
 53. Osmieri L, Monteverde Videla AHA, Armandi M, Specchia S (2016) Influence of different transition metals on the properties of Me–N–C (Me = Fe, Co, Cu, Zn) catalysts synthesized using SBA-15 as tubular nano-silica reactor for oxygen reduction reaction. *Int J Hydrogen Energy* 41:22570–22588.
 54. Osmieri L, Monteverde Videla AHA, Ocón P, Specchia S (2017) Kinetics of oxygen electroreduction on Me-N-C (Me = Fe, Co, Cu) catalysts in acidic medium: Insights on the effect of the transition metal. *J Phys Chem C* 121:17796–17817.
 55. Chen R, Li H, Chu D, Wang G (2009) Unraveling oxygen reduction reaction mechanisms on carbon-supported Fe-phthalocyanine and Co-phthalocyanine catalysts in alkaline solutions. *J Phys Chem C* 113:20689–20697.
 56. Goenaga GA, Roy AL, Cantillo NM, et al (2018) A family of platinum group metal-free catalysts for oxygen reduction in alkaline media. *J Power Sources* 395:148–157.
 57. Chlistunoff J (2011) RRDE and voltammetric study of ORR on pyrolyzed Fe/polyaniline catalyst. on the origins of variable Tafel slopes. *J Phys Chem C* 115:6496–6507.
 58. Santori PG, Speck FD, Li J, et al (2019) Effect of pyrolysis atmosphere and electrolyte pH on the oxygen reduction activity, stability and spectroscopic signature of FeN_x

moieties in Fe-N-C catalysts . J Electrochem Soc 166:F3311–F3320

- 1
2
3 59. Lee JS, Park GS, Kim ST, et al (2013) A highly efficient electrocatalyst for the oxygen
4 reduction reaction: N-doped ketjenblack incorporated into Fe/Fe₃C-functionalized
5 melamine foam. Angew Chemie - Int Ed 52:1026–1030.
6
7
- 8
9 60. Kim JH, Sa YJ, Jeong HY, Joo SH (2017) Roles of Fe–N_x and Fe–Fe₃C@C species in
10 Fe–N/C electrocatalysts for oxygen reduction reaction. ACS Appl Mater Interfaces
11 9:9567–9575.
12
13
- 14
15 61. Gokhale R, Chen Y, Serov A, et al (2016) Direct synthesis of platinum group metal-free
16 Fe-N-C catalyst for oxygen reduction reaction in alkaline media. Electrochem commun
17 72:140–143.
18
19
20
21
22
23
24
25
26
27
28
29
30
31
32
33
34
35
36
37
38
39
40
41
42
43
44
45
46
47
48
49
50
51
52
53
54
55
56
57
58
59
60
61
62
63
64
65



Click here to access/download
Supplementary Material
Revised SI.docx



